Influence of High Electric Field on Operation of AlGaN/AlN/GaN High Electron Mobility Transistor

M. Glinkowski*, B. Paszkiewicz and R. Paszkiewicz

Faculty of Microsystem Electronics and Photonics,
Wrocław University of Science and Technology, Janiszewskiego 11/17, 50-370 Wrocław, Poland

Received: 05.02.2020 & Accepted: 05.07.2021

Doi: 10.12693/APhysPolA.140.192 *e-mail: mateusz.glinkowski@pwr.edu.pl

In AlGaN/AlN/GaN heterostructures, as a result of spontaneous and piezoelectric polarization with the occurrence of donor surface states, a triangular potential well is formed on the interface, filled with two-dimensional electron gas with a concentration of 10^{13} cm^{-2} and a mobility of 2000 cm^2/(V s). An increase of the potential in the channel of an AlGaN/AlN/GaN high electron mobility transistor, caused by the flow of the drain current, results in: a decrease of the two-dimensional electron gas concentration, an increase of electric field and an increased drift velocity of electrons. At the drainage end of the gate, the electrons reach their maximum drift velocity which is correlated with the material limitations. Consequently, a rapid nonlinear increase of the channel potential, a decay of the two-dimensional electron gas channel, and pushing of the electrons towards the buffer occurs. The vertical current component starts to increase then while the horizontal current component decreases. Moreover, between the gate and the drain electrodes the two-dimensional electron gas channel is gradually rebuilt due to the presence of a low electric field. The Advanced Physical Models of Semiconductor Devices software was used to simulate these phenomena in the structure of an AlGaN/AlN/GaN high electron mobility transistor.

topics: APSYS, AlGaN/GaN, HEMT, simulation

1. Introduction

Unique properties of gallium nitride [1] mean that it is now in demand to supplement silicon technology. To achieve this goal, semiconductor materials from $A^{III}B^{V}$ group have been of great interest to researchers since the 1980s [2]. This group includes the AlGaN/AlN/GaN type high electron mobility transistor (HEMT) heterostructures [3]. The technology of AlGaN/AlN/GaN type HEMT heterostructures involves the metal organic chemical vapor epitaxy (MOVPE) technique [4–6] for the fabrication of the devices.

Two-dimensional electron gas (2DEG) resulting from the charges introduced by spontaneous and piezoelectric polarization [7, 8] combined with the donor surface states [9, 10] forms a conductive channel in AlGaN/AlN/GaN HEMTs. During the operation of an AlGaN/AlN/GaN type HEMT heterostructure, the key role is played by the electron drift velocity, which varies with the electric field in GaN [11–13].

The transport properties are also influenced by the increase of the temperature resulting from self-heating effects [14–16]. The role and influence of a high electric field on transport properties in AlGaN/GaN has been extensively studied [17–29].

To study the transport properties of AlGaN/AlN/GaN type HEMT heterostructure in high electric field, advanced physical models of semiconductor devices (APSYS) simulations were performed. A rapid increase of the potential in the channel was observed, caused by the current flow from source to drain and the saturation of electron drift velocity. This study reveals that the electrons from the quantum well are pushed towards the buffer and the 2DEG channel has to temporarily disappear in order to satisfy Kirchhoff's first law.

2. AlGaN/AlN/GaN type HEMT heterostructures

The schematic drawing of the simulated AlGaN/AlN/GaN type HEMT heterostructure is shown in Fig. 1. The 2DEG channel is formed in the 2 μm GaN buffer layer, which is separated from a 20 nm AlGaN barrier by a 2 nm thin AlN spacer. The channel is created as a result of the compensation of charges of the donor surface states with charges introduced by the spontaneous and piezoelectric polarization. The donor surface states, with the concentration of 10^{14} cm^{-2}, are placed 0.4 eV above the conduction band [30].

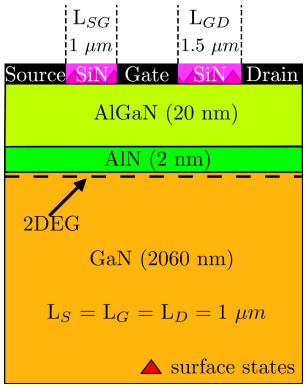

Fig. 1. Schematic drawing of a basic AlGaN/AlN/GaN type HEMT heterostructure. Source to gate distance $L_{SG} = 1$ μm, gate to drain $L_{GD} = 1.5$ μm. Length of source/gate/drain electrodes is 1 μm. Size of the structure is $L = 5.5$ μm. Surface states (red triangles) with energy of 0.4 eV are passivated by SiN.

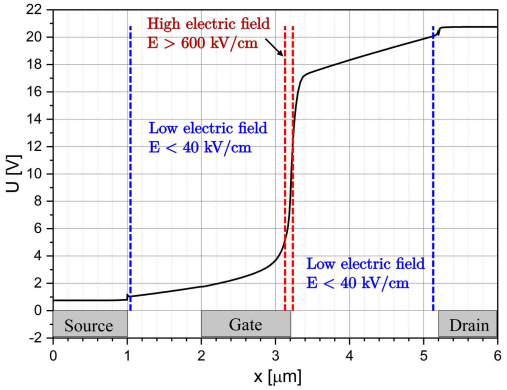

Fig. 2. The distribution of potential in the channel of AlGaN/GaN HEMT. The 1D GCA model and 2D Poisson equations were used in the low and high electric field region, respectively.

The area between the source (S), gate (G), and drain (D) electrodes is passivated by SiN material. The distance between the source and gate electrodes is equal to $L_{SG} = 1$ μm and the distance between the gate and drain electrodes corresponds to $L_{GD} = 1.5$ μm. The measured length of each electrode is 1 μm. Therefore, the size of the whole structure amounts to $L = 5.5$ μm. This kind of structure allows us to obtain a high drain current and it ensures repeatability by using UV lithography.

3. Transport in low and high electric field

The distribution of potential in the channel is shown in Fig. 2. Between the source and gate contacts, the potential increases linearly according to Ohm's law. Beneath the gate electrode, the potential starts to increase nonlinearly due to a nonlinear increase of drift velocity, similarly as in the GaN material. When the electrons reach their maximum drift velocity, to satisfy the current continuity, the potential has to increase rapidly. Due to the very high electric field ($E > 600$ kV/cm), electrons will leave the channel because they are pushed towards the buffer layer where electrons possess bulk GaN mobility.

In the area between the gate and drain electrodes, the potential obeys Ohm's law again, therefore the electric field in this region decreases from high to low. As a result, the electrons will return to the channel. However, their mobility could be reduced due to the injection into the buffer and temporary decay of a quantum well.

It is possible to distinguish two characteristic regions. The first is where the drift velocity of electrons is proportional to the electric field and lower than their maximum value in GaN. In this low electric field region, a linear increase of potential along the channel (caused by the current flow from source to drain) will reduce the surface carrier concentration. Therefore, to calculate the surface electron concentration, it is essential to use the one-dimensional gradual channel approximation (1D GCA) model [31]:

$$n_s(x) = \frac{C_{\mathrm{Gch}}}{q}\Big(V_{\mathrm{G}} - V_{\mathrm{ch}}(x) - V_{\mathrm{p}}\Big), \tag{1}$$

where C_{Gch} is the gate–channel capacitance, q is the elementary charge, and V_{G}, V_{ch}, V_{p} are the potentials of gate, channel, and pinch-off voltage, respectively.

In the second region which is correlated with a high electric field, the electrons reach their maximum drift velocity, according to observations of negative differential resistance (NDR), in GaN [32]. A further increase of drift velocity is not possible, therefore the GCA model cannot be used in this region. The determination of concentration distribution requires then more sophisticated methods, for example two-dimensional Poisson equations [33]. Namely,

$$\frac{\partial^2\psi}{\partial x^2} + \frac{\partial^2\psi}{\partial y^2} = -\frac{1}{\varepsilon_0\varepsilon_s}\rho(x,y), \tag{2}$$

where $\psi(x,y)$ and $\rho(x,y)$ are the electric potential and charge density in x and y directions, ε_0 stands for the permittivity of vacuum, and ε_s is the static permittivity of GaN.

In the high electric field region, the 2DEG channel disappears, but the current continuity is still satisfied because of electrons flow through the undoped buffer.

For better understanding of the influence of high electric field on the operation of AlGaN/AlN/GaN HEMT the electron concentration was calculated at every point of the simulated heterostructure. The results are shown in Fig. 3. The electron concentration is presented in a logarithmic scale with units of cm^{-3}. Source, gate and drain electrodes are marked as S, G, and D, respectively. For clarity — the SiN passivation is shown in the inset of Fig. 3 only.

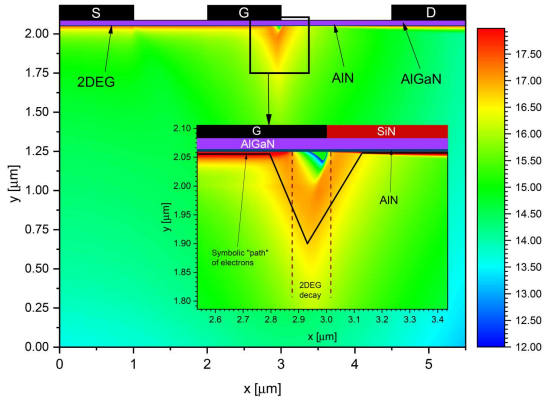

Fig. 3. Electron concentration n [cm^{-3}] in AlGaN/AlN/GaN HEMT, U_{DS} = 20 V and U_{GS} = 0 V. The black line shows a symbolic "path" of the electrons from the source towards the drain electrode.

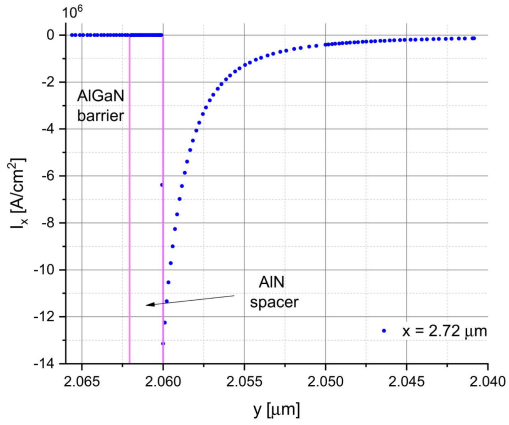

Fig. 4. Horizontal current near the drainage end of the gate at $x = 2.72$ μm.

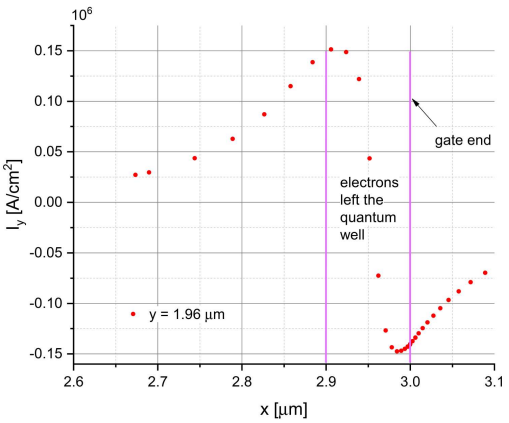

Fig. 5. Vertical current near the drainage end of the gate at $y = 1.96$ μm.

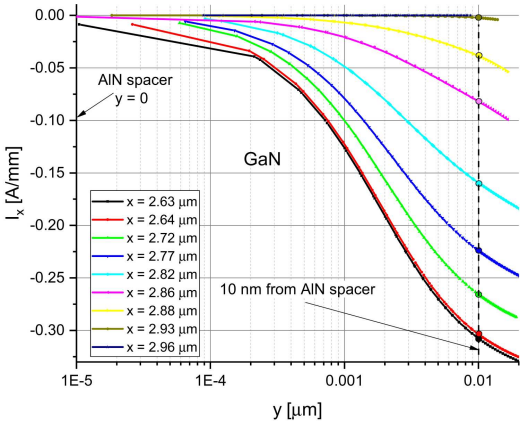

Fig. 6. Integrated horizontal current component near the drain end of the gate from cross-sections in different points at the AlGaN/AlN/GaN heterostructure.

It is clear that the whole GaN buffer layer is half-insulating, due to the presence of electrons in the range of 10^{12} to 10^{19} cm^{-3}. In the inset of Fig. 3 a symbolic "path" of the electrons from source towards the drain electrode is shown. Due to the presence of a high electric field the electrons are pushed towards the buffer layer (a current in the y direction starts to increase while that in the x direction decreases). At the drain end of the gate electrode where the quantum well is disappearing, the electrons stop being quantized in the y direction and start to spread into the buffer, reaching the typical value of mobility in GaN.

The current in the x and y directions near the drain end of the gate is shown in Figs. 4 and 5. Two horizontal dashed black lines highlight the region where the quantum well disappears and electrons are pushed into the buffer. The horizontal current component (see Fig. 4) values were evaluated from a cross-section at $x = 2.72$ μm. Between the pink lines there is a 2 nm thin AlN spacer and on the left a part of an AlGaN barrier. The vertical current component values (see Fig. 5) were evaluated below the "quantum well" from a cross-section at $y = 1.96$ μm. It is apparent that the vertical current component starts to increase below the gate electrode and electrons are pushing towards the buffer layer (positive values). The maximum positive value in Fig. 5 corresponds to the decay of the quantum well. Subsequently electrons near the gate ends start moving in the opposite direction (negative values) and the process of rebuilding the quantum well will take place.

The region where the electrons leave the quantum well in Fig. 5 is marked by solid black lines. The vertical current component changes its sign which corresponds to its change of direction. At $x \approx 2.7$ μm the electrons start to leave the quantum well and at $x \approx 2.96$ μm they return to the 2DEG channel.

In order to calculate the current in the 2DEG channel at a different point below the gate electrode it is essential to integrate the horizontal current component shown in Fig. 4. The result of such an integration of the horizontal current component for nine different points is presented in Fig. 6. A dashed black line highlights the distance from the AlN spacer, here 10 nm, near the end of the quantum well.

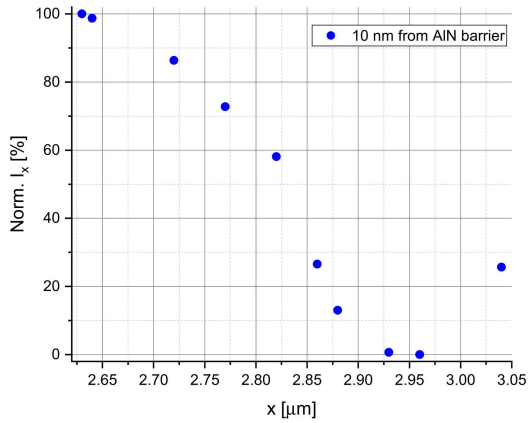

Fig. 7. Normalized value of current I_x evaluated for ten points of cross-sections.

Taking the value of current I_x at 10 nm from the AlN spacer for $x = 2.63$ nm as the reference value of the maximum current in the 2DEG channels (respectively far away from the high electric field region, where its impact is negligible), a normalized value of current I_x could be obtained. It is presented in Fig. 7.

4. Conclusion

The transport of the 2DEG in the channel of an AlGaN/AlN/GaN type HEMT heterostructures was studied. Kirchhoff's first law (current continuity, i.e., the current at the input of a device must equal the current at its output) has to be satisfied, therefore the 1D GCA and the 2D Poisson equations had to be used. It was found that the unintentionally doped buffer, which is normally an insulating material, becomes highly conductive due to the carrier injection from the channel during the operation of the device. Beneath the gate electrode, the transport of the 2DEG can be affected by trapping centers in the buffer or on the surface.

Acknowledgments

This work was co-financed by the National Centre for Research and Development grants TECHMATSTRATEG No. 1/346922/4/NCBR/2017, the Polish National Agency for Academic Exchange under the contract PPN/BIL/2018/1/00137 and the Wrocław University of Technology K70W12D02 subsidy. This work was accomplished thanks to the product indicators and result indicators achieved within the projects co-financed by the European Union within the European Regional Development Fund, through a grant from the Innovative Economy (POIG.01.01.02-00-008/08-05) and by the National Centre for Research and Development through the Applied Research Program Grant No. 178782 and Grant LIDER No. 027/533/L-5/13/NCBR/2014.

References

[1] M. Rais-Zadeh, A. Ansari, Y. Cordier, *J. Microelectromech. Syst.* **23**, 1252 (2004).

[2] T. Mimura, *Fujitsu Sci. Tech. J.* **54**, 3 (2018).

[3] H. Amano, Y. Baines, E. Beam et al., *J. Phys. D* **51**, 163001 (2018).

[4] M. Wośko, B. Paszkiewicz, T. Szymański, R. Paszkiewicz, *J. Cryst. Growth* **414**, 248 (2015).

[5] S. Owczarzak, A. Stafiniak, R. Paszkiewicz, *J. Vac. Sci. Technol. B* **37**, 1 (2019).

[6] M. Wośko, B. Paszkiewicz, A. Stafiniak, J. Prażmowska-Czajka, A. Vincze, K. Indykiewicz, M. Stępniak, B. Kaczmarczyk, R. Paszkiewicz, *Mater. Sci. Semicond. Process.* **107**, 104816 (2020).

[7] J.P. Ibbetson, P.T. Fini, K.D. Ness, S.P. DenBaars, J.S. Speck, U.K. Mishra, *Appl. Phys. Lett.* **77**, 250 (2000).

[8] O. Ambacher, B. Foutz, J. Smart et al., *J. Appl. Phys.* **87**, 334 (2000).

[9] B. Jogai, *J. Appl. Phys.* **93**, 1631 (2003).

[10] R. Vetury, *IEEE Trans. Electron Dev.* **48**, 560 (2001).

[11] J. Kolník, İ.H. Oğuzman, K.F. Brennan, *J. Appl. Phys.* **78**, 1033 (1995).

[12] U.V. Bhapkar, M.S. Shur, *J. Appl. Phys.* **82**, 1649 (1997).

[13] J.M. Tirado, J.L. Sánchez-Rojas, J.I. Izpura, *IEEE Trans. Electron Dev.* **54**, 410 (2007).

[14] V.O. Turin, A.A. Balandin, *J. Appl. Phys.* **100**, 054501 (2006).

[15] Xiao-Dong Wang, Wei-Da Hu, Xiao-Shuang Chen, Wei Lu, *IEEE Trans. Electron Dev.* **59**, 1393 (2012).

[16] G. Atmaca, P. Narin, E. Kutlu, T.V. Malin, V.G. Mansurov, K.S. Zhuravlev, S.B. Lisesivdin, E. Özbay, *IEEE Trans. Electron Dev.* **65**, 950 (2018).

[17] S. Rajasingam, J.W. Pomeroy, M. Kuball, M.J. Uren, T. Martin, D.C. Herbert, K.P. Hilton, R.S. Balmer, *IEEE Electron Dev. Lett.* **25**, 456 (2004).

[18] M.J. Uren, M. Caesar, S. Karboyan, P. Moens, P. Vanmeerbeek, M. Kuball, *IEEE Electron Dev. Lett.* **36**, 826 (2015).

[19] Jianhua Liu, Yufeng Guo, Jun Zhang, Jiafei Yao, Xiaoming Huang, Chenyang Huang, Zhi Huang, Kemeng Yang, *Superlatt. Microstruct.* **138**, 106327 (2020).

[20] Luoyun Yang, Baoxing Duan, Yandong Wang, Yintang Yang, *Superlatt. Microstruct.* **128**, 349 (2019).

[21] Wei Mao, Ju-Sheng Fan, Ming Du, Jin-Feng Zhang, Xue-Feng Zheng, Chong Wang, Xiao-Hua Ma, Jin-Cheng Zhang, Yue Hao, *Chin. Phys. B* **25**, 127305 (2016).

[22] M. Matys, K. Nishiguchi, B. Adamowicz, J. Kuzmik, T. Hashizume, *J. Appl. Phys.* **124**, 224502 (2018).

[23] M.J. Anand, G.I. Ng, S. Arulkumaran, C.M. Manoj Kumar, K. Ranjan, S. Vicknesh, S.C. Foo, B. Syamal, X. Zhou, *Appl. Phys. Lett.* **106**, 083508 (2015).

[24] R.R. Chaudhuri, V. Joshi, S.D. Gupta, M. Shrivastava, in: *2020 32nd Int. Symposium on Power Semiconductor Dev. and ICs (ISPSD)*, 2020, p. 341.

[25] S. Gupta, J.K. Kaushik, A. Gupta, V. Kumar, V.R. Balakrishnan, *Semiconduct. Sci. Technol.* **35**, 085035 (2020).

[26] Luoyun Yang, Baoxing Duan, Yandong Wang, Yintang Yang, *Superlatt. Microstruct.* **128**, 349 (2019).

[27] L. Ardaravičius, A. Matulionis, J. Liberis, O. Kiprijanovic, M. Ramonas, L.F. Eastman, J.R. Shealy, A. Vertiatchikh, *Appl. Phys. Lett.* **83**, 4038 (2003).

[28] Hao Zou, Lin-An Yang, Xiao-Hua Ma, Yue Hao, *Superlatt. Microstruct.* **152**, 106843 (2021).

[29] Jianhua Liu, Yufeng Guo, Jun Zhang, Jiafei Yao, Xiaoming Huang, Chenyang Huang, Zhi Huang, Kemeng Yang, *Superlatt. Microstruct.* **138**, 106327 (2020).

[30] G. Koley, M.G. Spencer, *J. Appl. Phys.* **90**, 337 (2001).

[31] J.P. Colinge, *IEEE Trans. Electron Dev.* **37**, 718 (1990).

[32] J.D. Albrecht, R.P. Wang, P.P. Ruden, M. Farahmand, K.F. Brennan, *J. Appl. Phys.* **83**, 4777 (1998).

[33] B. Mebrate, P.R. Koya, *Am. J. Appl. Math.* **3**, 297 (2015).